Rice Disease Detection by Image Analysis

Sudarshan S. Chawathe
School of Computing and Information Science & Climate Change Institute
University of Maine
Orono, Maine 04469-5711, USA
chaw@eip10.org

***Abstract*—This paper provides a method for automatically classifying diseases in rice plants by analyzing photographs of rice leaves. The method uses image processing algorithms to detect leaves and likely disease-induced lesions in the leaves. Next, several attributes are computed based on the dimensions of leaves and lesions, the numbers and shapes of lesions, as well the color characteristics of lesions and intact portions of leaves. These attributes are used to build classification models using well established algorithms. The method is evaluated using a publicly available database of rice leaf images.**

***Index Terms*—Rice Disease, Rice Leaf, Image Processing, Classification, Machine Learning.**

I. Introduction

Rice is one of the most important crops worldwide and diseases that affect rice plants have major impacts on large segments of the world population. Early and accurate detection of rice (plant) diseases allows corrective action that reduces the negative impact. However, such disease detection by human experts is time-consuming and does not scale because a human can examine only a very limited number of plants carefully. Therefore, automated methods for rice disease detection provide an important step toward addressing this important problem.

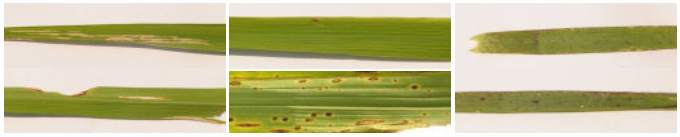

Fig. 1. Sample images of leaves of rice plants affected by various diseases: *bacterial leaf blight* (leftmost two), *brown spot* (middle two), and *leaf smut* (rightmost two). Images are extracted from a dataset of images from prior work [1], [2].

This paper addresses the problem of detecting and categorizing rice plant diseases using photographic images of the leaves of rice plants. In more detail, the input consists of images similar to the samples depicted in Fig. 1. The desired output is a determination of the disease afflicting the photographed plant. As described in more detail later, the problem is challenging because the differences in the visual appearances of leaves afflicted with different diseases can be subtle and, further, they can be overshadowed by visual artifacts such as shadows, light glare, color tinting, background noise, low resolution, etc.

This paper's method for solving this problem consists of three phases. In the first phase, the image is analyzed using a carefully designed pipeline of image-processing operations, with the goal of accurately identifying leaves and lesions (caused by disease). The second phase computes several attributes (features) based on the number, size, shape, and color of the leaf and lesions identified in the previous phase. The third phase uses well established classification algorithms to infer the disease from the attribute-values determined by the second phase. This three-phase process is performed once on a suitable corpus of images in order to train the models. Subsequently, the learned models are used for classification of unknown images (using the same three phases).

The main *contributions* of this paper:

- It describes and motivates the problem of detecting rice diseases using photographic images and outlines a three-phase method for addressing it.
- It presents an image-processing pipeline that is effective at detecting lesions in leaves. This pipeline is the result of extensive experimentation with numerous alternative approaches.
- It describes a set of attributes (features) that may be extracted from leaf images (after image processing) that provide a good basis for further classification work.
- It summarizes the results of an experimental evaluation of the described methods on a publicly available dataset from prior work [1], [2].

The primary *results*:

- The image-processing methods noted above are effective at correctly identifying almost all lesions in leaves.
- The extracted attributes in combination with well established classification algorithms provide competitive accuracy using metrics such as percent correctly classified and the F measure.
- The disease-detection method is very computationally efficient during both training (model building) and testing (disease detection).
- Using metric-based attribute-selection, the number of attributes needed for classification can be significantly reduced, providing significant improvement in efficiency and simplicity at the cost of only a small drop in accuracy.

Outline: The image-processing steps used to delineate leaves and lesions are described in Section II. The numerical attributes extracted from the lesions thus identified are

978-1-7281-3783-4/20/$31.00 ©2020 IEEE

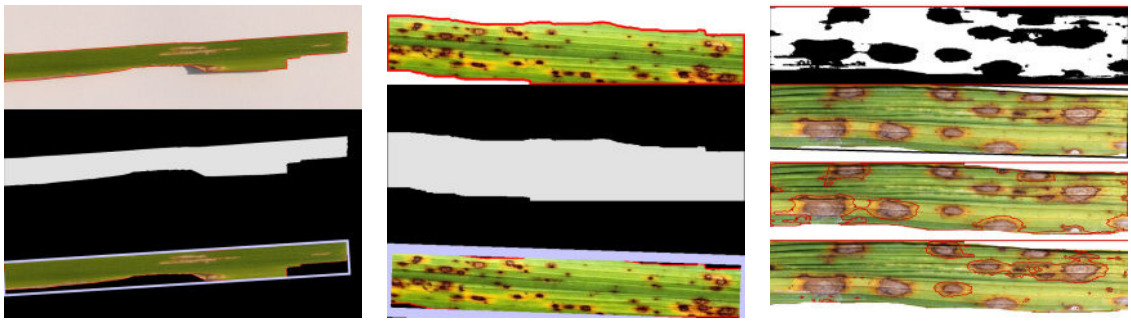

Fig. 2. Masking and measuring and two different image resolutions (left and middle). The thickness of the light blue circumscribing rectangle is the same in both images. Detecting lesions using contours (right).

described in Section III. Section IV summarizes the results of a detailed experimental evaluation of these methods. Methods for reducing the required number of attributes are outlined in Section V. Related work is addressed by Section VI, while Section VII summarizes the paper and outlines ongoing and future work.

II. Leaf and Lesion Localization

Since the resolution and scale (magnification) of photographed rice leaves may vary significantly (as is the case in the test dataset—cf. Figs. 2 and 2), it is important to normalize attributes (such as areas of lesions) to factor out variations due to the image's scale. This paper's method for this task uses a *preliminary* identification of the approximate leaf region based on color. Fig. 2 illustrates this step being used to generate the preliminary leaf-mask (middle image) from the input image (top). Next, a rectangle is fitted to the leaf thus identified, as illustrated by the bottom image in Fig. 2. The smaller side of this rectangle (corresponding to leaf width) is used as the scale factor for normalizing lengths and areas computed later. It is important to note that this simple color-based leaf detection is used solely for determining the scale. A more accurate method for delineating leaves is described later.

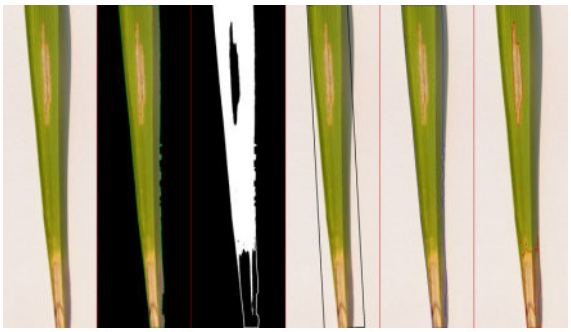

Fig. 3. An example of a confusing shadow.

At first consideration, it may seem that lesions in leaves may be detected simply using color, since the lesions have a hue that is typically significantly distant from the predominant green of the leaves. However, the situation is more complicated due to the interaction of image artifacts such as shadows, over-exposed portions (that may be confused with the background) with the lesions. Fig. 2 illustrates one such complication. Only a few of the obvious lesions in the image are detected using a simple color-based contour due to the leaf boundary impinging on many of the lesions. Fig. 3 illustrates another complication, due to shadows. Here a portion of the leaf that is afflicted by a light colored lesion is confounded with the similarly light colored background, resulting in the leaf being inaccurately delineated and one lesion being missed. The other, which is fully enclosed within the leaf boundary, is detected.

In order to address such complications, the method used here performs multiple phases of color-based segmentation and contour detection. The largest contour detected after the first color-based segmentation is used to compute an initial mask for the approximate leaf area. This mask is subjected to blurring (Gaussian kernel of size 21×21) followed by morphological completion (using a rectangular structuring element of size 3×3) and erosion (three iterations using a rectangular structuring element of size 11×11) to yield a more refined leaf region. Further, in order to ameliorate edge-related difficulties, a leaf-green colored border is drawn on the leaf image for use by subsequent steps.

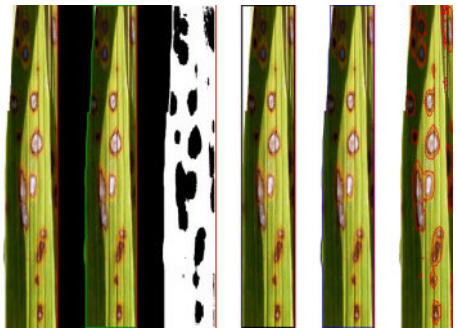

Fig. 4. An example of a confusing shadow that is successfully interpreted.

This refined method is successful at detecting leaves and lesions in several challenging cases. Fig. 4 depicts a case that includes a very dark shadow that covers part of the leaf, making it difficult even for a human to quickly determine the

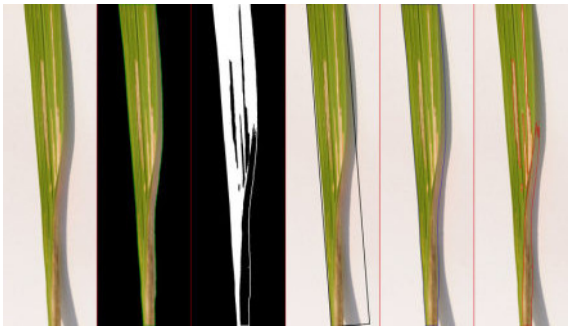

Fig. 5. An example of a lesion along an edge in addition to a confusing shadow that is successfully interpreted.

leaf boundary. However, the above method is successful at not only identifying the leaf accurately but also at identifying the lesions (including the parts that are in the deep shadow). Fig. 5 depicts another challenging case, where there is not only a shadow, which makes it hard to determine the lower edge of the leaf, but also a long and large lesion that borders the very same leaf edge. Again, the above method is successful at identifying both the leaf and the troublesome lesion here.

III. Attribute extraction

Table I summarizes the numerical attributes (features) that are extracted for use in classification, following the leaf and lesion identification of the previous section.

Two attributes are special cases: The `id` attribute identifies the source image file for debugging and tracing purposes and is not used in the subsequent classification. The `disease` attribute is the nominal class attribute that is the target of detection.

The remaining attributes may be divided into five categories, as demarcated by the lines in Table I. The first category includes two simple counts: the number of lesions and the number of lesions that enclose a nonempty area. The latter is notable because visual artifacts sometimes result in a number of tiny spots being marked as lesions, but these have zero area and may thus be separated.

The second category of attributes is based on the aspect ratios of the lesions. Attention to aspect ratios is motivated by the observation that some diseases, such as bacterial leaf blight (top two images in Fig. 1) are characterized by long and narrow lesions while others, such as brown spot (middle two images in Fig. 1) produce more rounded lesions. In particular, we compute the mean and and standard deviation of normalized areas, as well as the areas of the five smallest and five largest lesions. If there are fewer than five, the corresponding attributes are set to zero.

The third category of attributes is based on the areas enclosed by the lesions. These areas are normalized using the square of the leaf width as computed by the earlier preliminary leaf-detection phase. The specific attributes are noted in Table I and are very similar to those used for the aspect ratios above.

The fourth category of attributes uses the well-known image moments (of the geometric kind) [**?**] applied to the areas enclosed by lesions. The (i, j)'th moment of an image (or matrix) is defined as follows, using $s(x, y)$ to denote the value of the pixel (or cell) at location (x, y): $M_{ij} = \sum_x \sum_y x^i y^j s(x, y)$ where the summations are taken over the range of x and y values in the image or matrix. This definition is generalized to apply to a specified region of interest $\mathcal{R}$ (e.g., a lesion in the current work) instead of the entire image by limiting the summation to points in the region: $M_{ij}(\mathcal{R}) = \sum_{(x,y)\in\mathcal{R}} x^i y^j s(x, y) = \sum_x \sum_y x^i y^j s(x, y) \cdot m_{\mathcal{R}}(x, y)$ where $m_{\mathcal{R}}$ is a mask for region $\mathcal{R}$. We use the ten M_{ij} moments listed in the table, for each of the five largest lesions, yielding 50 attributes. A similar computation is also performed for the five smallest lesions (with nonzero area), yielding another 50 attributes.

The fifth and final category of attributes is based on color; specifically, the color of the leaf background, the lesions, and their difference. In more detail, we compute the mean and standard deviation of each of the three color components (hue, saturation, value) for both the leaf background and the lesions, and also for their difference, yielding $2 \times 3 \times 3 = 18$ color-based attributes.

IV. Implementation and Experimental evaluation

The attributes described in the previous section form the basis of the classification phase, which uses well established algorithms, such as Random Forest, Logistic Model Trees, and Sequential Minimal Optimization for Support Vector Machines.

The implementation is written in the Kawa Scheme language and runs on the OpenJDK Java Virtual Machine (JVM). It uses OpenCV for the low-level image-processing operations of the first two phases described in Sections II and III (leaf and lesion identification, and attribute extraction) and the WEKA workbench for the third phase (classification).

The classification algorithms used in the study include ZeroR and OneR to serve as baselines, three other rule-based algorithms (such as PART, Decision Table, and JRip), five tree-based algorithms (J48, Random Forest, LMT, Random Tree, and REP Tree), three function-based algorithms (SMO, Simple Logistic, and Logistic) , three Bayesian methods (Naive Bayes, Bayes Net with limited parents, and Bayes Net with unlimited parents), and three lazy methods (IBk, KStar, LWL). The experimental study uses conventional 10-fold cross-validation and a large number of trials so as to yield small deviations. Error bars in the bar graphs summarizing the results represent the standard error of the mean and are typically too small to discern.

In addition to the complete set of attributes described in the previous section and Table I, classification is also evaluated on different subsets of those attributes, as identified by the color-coded bars and legends in the charts, and detailed in Table II.

Fig. 6 summarizes the accuracy of classification quantified using the percentage of correctly classified instances (correctly identified diseases). Fig. 7 summarizes similar results on accuracy using the F-measure. Results for other metrics, such as

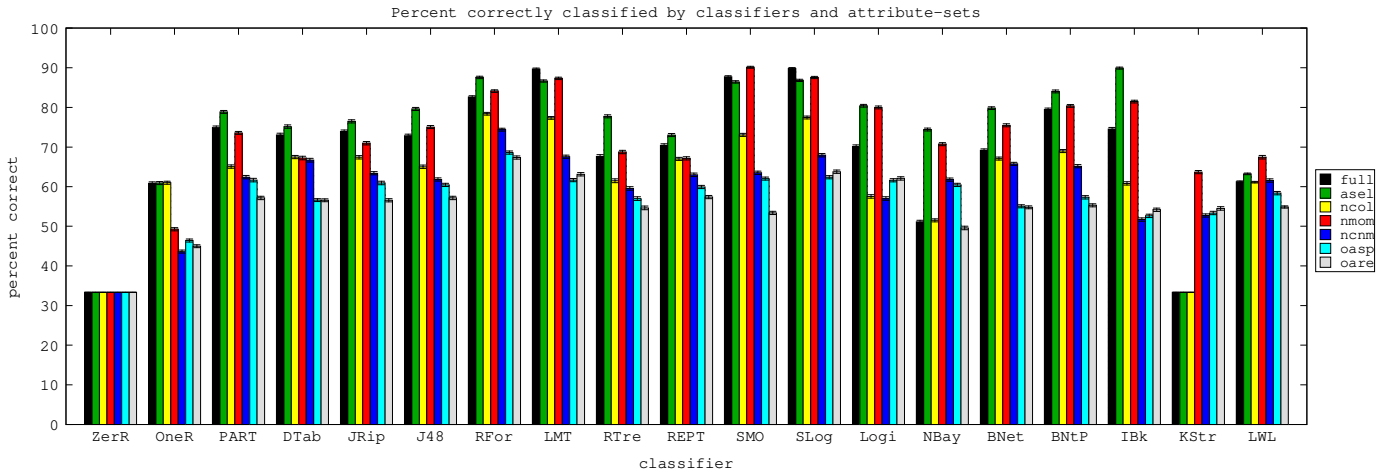

Fig. 6. Classification accuracy (percent correct) by classifier (groups labeled on horizontal axis) using various sets of attributes (individual color-coded bars with codes in the legend on the right corresponding to those in Table II).

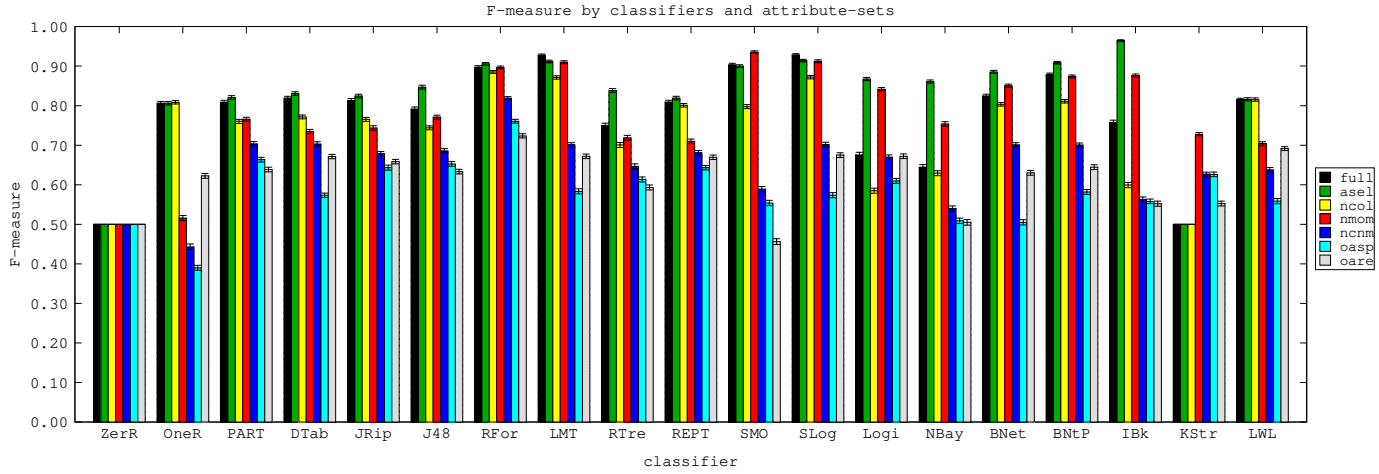

Fig. 7. F-measure by classifier using various sets of attributes. Other details are as in Fig. 6.

area under the receiver operating characteristic (ROC) curve, are qualitatively similar and are omitted here for brevity.

Fig. 8 summarizes the results on time required to train the models (learning time) for combinations of classification algorithms and attribute-sets. The results for testing times (classification times) are all extremely small, with the largest testing time being less than 1 ms and most substantially lower. Those results are therefore omitted here for brevity.

V. Attribute Selection

It is often beneficial to reduce the number of attributes used for classification in order to improve performance. For this purpose, attributes may be selected using a few different metrics. Here we present the results of the experimental computation of two metrics from the attributes of Table I: a metric based on the OneR classifier (Fig. 10) and another conventional one based on Information Gain (Fig. 11). We may note that the `h0m01` attribute is ranked high by both metrics. Recall, from Table I, that this attribute measures the M_{01} moment of the largest-area lesion. Several other moments of the largest- and smallest-area lesions are also featured prominently by both metrics. We may note also that attribute merit drops off much more rapidly when using the Information Gain metric.

These observations suggest that accurate classification may be achieved using a small subset of the full complement of 144 attributes used earlier. For this purpose, the use of the well-known Correlation-based Feature Subset Selection method yields the following set of 17 attributes, which are denoted by `asel` in the experimental results of Section IV: `smin0 smax0 smax2 asdev amin4 h0m00 h0m01 h0m02 h0m10 l1m02 cbhmn cbsmn cbssd cbvmn cbvsd cdsmn cdvmn`.

VI. Related Work

The task of image segmentation, as used by the first phase of this paper's method, may be performed using diverse approaches, such as feature-based fuzzy rules [3], self-organizing neural networks [4], and wavelet filters [5]. A thresholding method similar to the method used to generate the initial

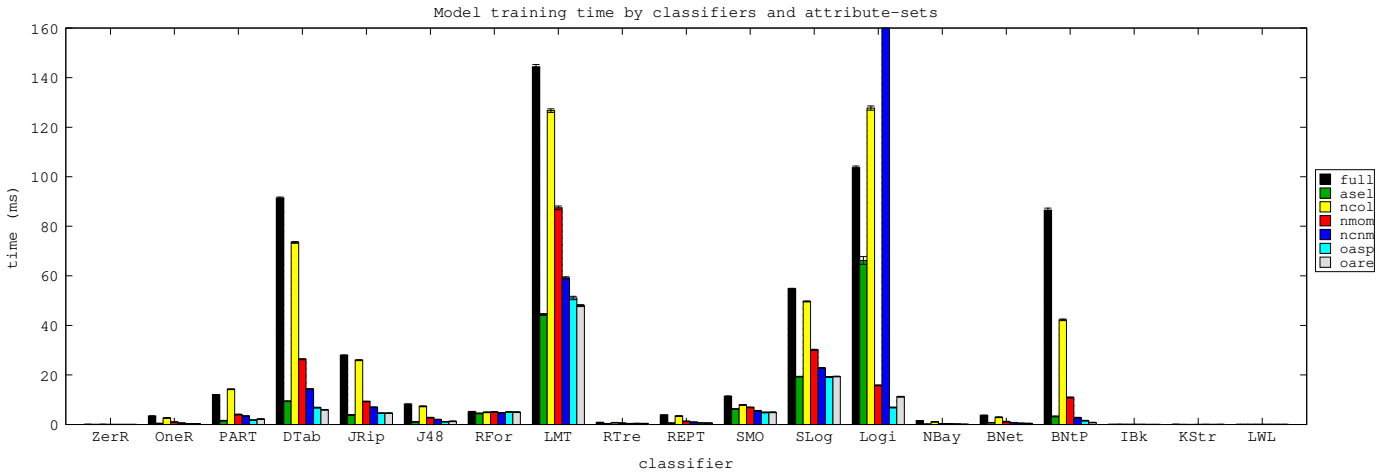

Fig. 8. Model training (learning) times by classifier using various sets of attributes. The out-of-range value for `Logi` and `ncnm` is 1191. Other details are as in Fig. 6.

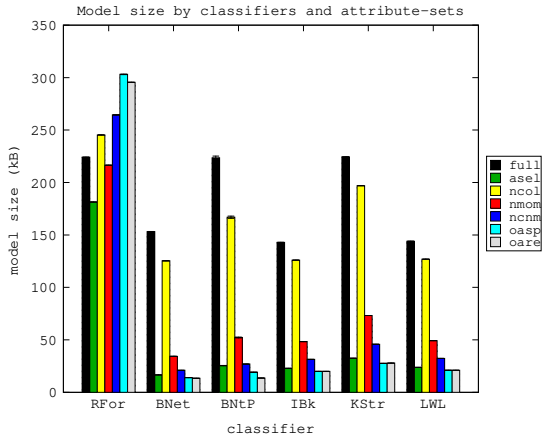

Fig. 9. Serialized sizes of learned models by classifier using various sets of attributes. The sizes for the algorithms not depicted here (for brevity) are all well below 40 kB. Other details are as in Fig. 6.

(approximate) leaf boundary in Section II has been used to detect brain tissues in CT images [6]. If the leaf images include substantial noise then denoising methods, such as those based on quadrature mirror filters [7], are likely to be a useful preprocessing step. Feature extraction is often a key part of image and video processing [8]. Recent work on feature reduction using genetic algorithms [9] is related to the attribute selection studied in Section V and could serve as an alternative method for that task.

There is a large body of work on detecting human diseases using diverse image processing methods. For example, some recent work uses multiscale uniform local binary pattern descriptors and other features for detecting diabetic retinopathy in images of retinas [10].

Deep learning methods have been very successful in image recognition (e.g., [11]) and it should be interesting to study their application to the problem of detecting rice plant diseases. Deep convolutional neural networks (DCNNs) have been recently applied to the tasks of detecting skin cancer in images of skin lesions [12] and identifying emotions [13], and to biometric user identification using electrocardiograms [14].

The Random Forest classification algorithm, which performs well on the classification tasks of this work (Section IV) is often the algorithm of choice [15]. The similar and, in some cases, better accuracy of other algorithms in Section IV, such as Logistic Model Trees (LMT) and Simple Logistic, is more notable here.

Recent work on improving the performance of machine learning in a distributed setting [16] may be used in a deployment of the method of this paper to smart-phones [17] and other low-power devices. The server and middleware parts of such a deployments would benefit from recent work on software engineering techniques to improve parallelizability [18]. Similarly, work on database services [19] and Web services [20] may be used to reduce the burden of the computing infrastructure in such a deployment.

VII. Conclusion

Automated detection of rice plant diseases is an important problem given the importance of rice as a worldwide crop. The work described here demonstrates the feasibility of rice disease detection using simple photographic images that may be collected in the field using smart-phone cameras or other easily available hardware. Image characteristics such as shadows, leaf damage unrelated to disease, over- and under-exposed areas, color variations, and lesions that abut leaf edges pose several challenges to accurate delineation of leaves and lesions. However, by using the carefully designed sequence of image-processing operations described in this paper, it is possible to successfully identify lesions even in challenging situations such as those illustrated by Figs. 4 and 5. A judicious collection of numerical attributes computed from characteristics of the leaves and lesions thus identified serves as the basis for the classification phase for disease identification. The experimental evaluation indicates that competitive

TABLE I
ATTRIBUTES EXTRACTED FROM PROCESSED IMAGE.

category code	count	description
`id`	1	source file identifier (not used for classification)
Lesion counts		
`les`	1	normalized number of lesions
`nz`	1	normalized number of lesions that enclose a nonzero area
Lesion aspect ratios		
`smean`	1	mean of the aspect ratios of lesions
`ssdev`	1	standard deviation aspect ratios of lesions
`smin`i	5	for $i = 0, \ldots, 4$, the five smallest aspect ratios of lesions (0 padded).
`smax`i	5	for $i = 0, \ldots, 4$, the five largest aspect ratios of lesions (0 padded).
Lesion areas		
`amean`	1	mean of the areas of lesions
`asdev`	1	standard deviation areas of lesions
`amin`k	5	for $k = 0, \ldots, 4$, the five smallest normalized areas of lesions (0 padded).
`amax`k	5	for $k = 0, \ldots, 4$, the five largest normalized areas of lesions (0 padded).
Lesion moments		
`h`k`m`ij	50	The standard M_{ij} moments of the k'th largest-area lesion, $k = 0, \ldots, 4$: M_{00}, M_{01}, M_{02}, M_{03}, M_{10}, M_{11}, M_{12}, M_{20}, M_{21}, M_{30}.
`l`k`m`ij	50	similar to above, but for the five lesions with the smallest areas
Leaf&lesion color		
`cbhmn`	1	mean (mn) hue (h) for color (c) of the leaf background (b)
`cbhsd`	1	standard deviation (sd) HSV hue (h) for color (c) of the leaf background (b)
`cbsmn`	1	similar to `cb`**`h`**`mn` but for the HSV color saturation (s) component instead of hue
`cbssd`	1	similar to `cb`**`h`**`sd` but for saturation (s)
`cbvmn`	1	similar to `cb`**`h`**`mn` but for the HSV color value (v) component instead of hue
`cbvsd`	1	similar to `cb`**`h`**`sd` but for value (v)
`clhmn`	1	similar to `c`**`b`**`hmn` but for the leaf lesions (l) instead of leaf background.
`clhsd`	1	similar to `c`**`b`**`hsd`, as above
`clsmn`	1	similar to `c`**`b`**`smn`, as above
`clssd`	1	similar to `c`**`b`**`ssd`, as above
`clvmn`	1	similar to `c`**`b`**`vmn`, as above
`clvsd`	1	similar to `c`**`b`**`vsd`, as above
`cdhmn`	1	similar to `c`**`b`**`hmn` but for the difference (d) between the leaf and lesion color components
`cdhsd`	1	similar to `c`**`b`**`hsd`, as above
`cdsmn`	1	similar to `c`**`b`**`smn`, as above
`cdssd`	1	similar to `c`**`b`**`ssd`, as above
`cdvmn`	1	similar to `c`**`b`**`vmn`, as above
`cdvsd`	1	similar to `c`**`b`**`vsd`, as above
`disease`	1	nominal class attribute
`Total`	146	(including class attribute and unused `id`)

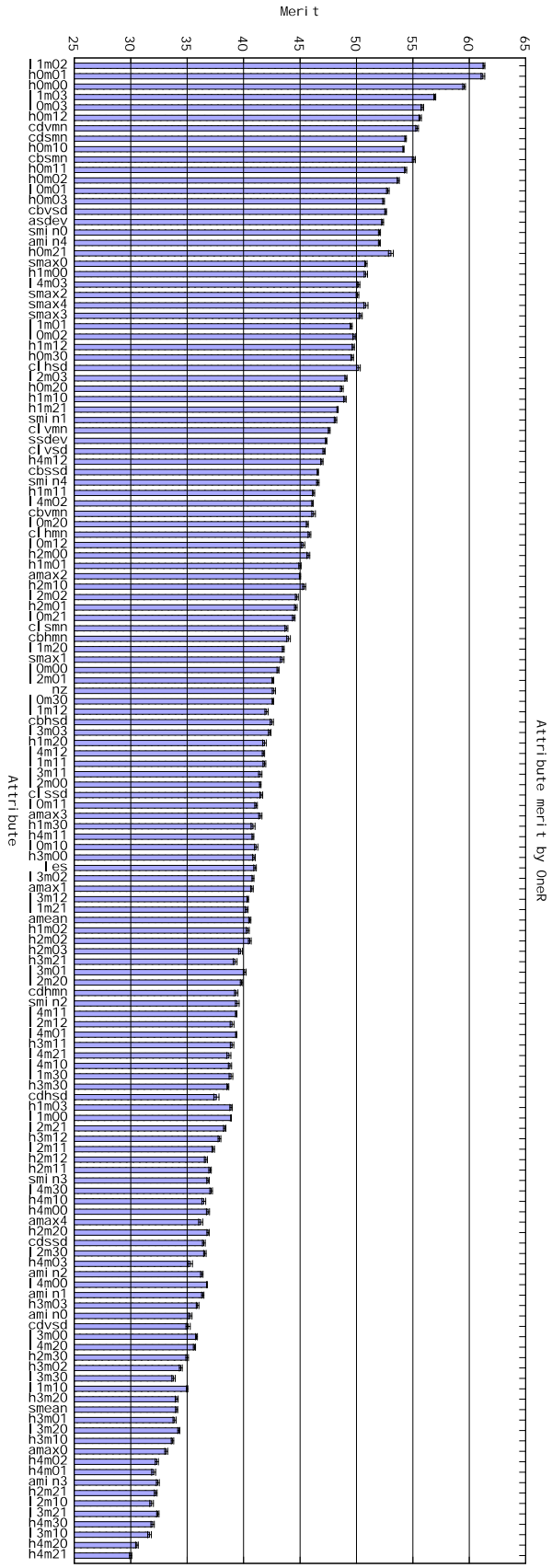

Fig. 10. Attribute merit using the OneR classifier.

TABLE II
ATTRIBUTE-SETS USED IN EXPERIMENTS. SEE TABLE I.

code	attribute-set
full	all attributes from Table I
asel	attributes produced by attribute-selection, Section V
ncol	(no color) all attributes other than color-based ones
nmom	(no moments) all attributes other than those based on image moments
ncnm	all attributes except those based on color or moments
oasp	(only aspect-ratios) only attributes based on lesion aspect ratio
oare	(only area) only attributes based on lesion areas

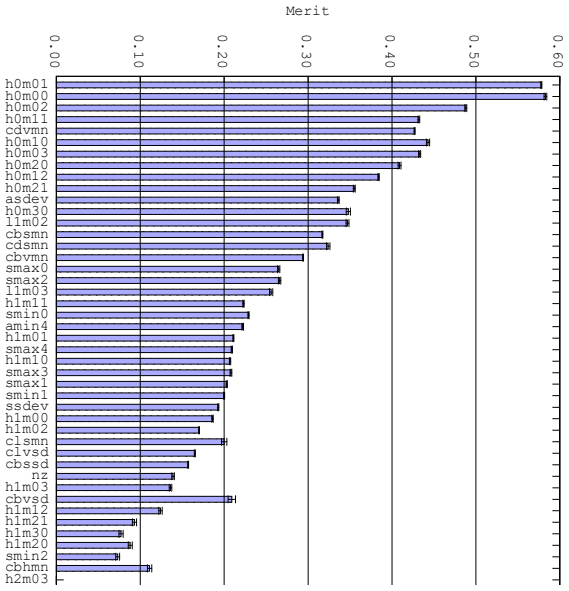

Fig. 11. Attribute merit using the Information Gain metric. For brevity, unlike Fig. 10, *only the high-scoring attributes are depicted*. Also unlike Fig. 10, most of the omitted ones have zero merit scores.

performance (compared with prior work) is achievable at very low computation cost.

Ongoing work is investigating further refinement of the image-processing phase by a careful examination of the misclassified instances. It is also expanding the work to more diverse datasets. In particular, it should be interesting to study datasets with a larger collection of disease and non-disease states.

ACKNOWLEDGMENTS

The presentation benefited from detailed reviews. This work was supported in part by the US National Science Foundation grants 1027960, 1142007, and 1848747, and was enabled by the dataset provided by prior work [1], [2].

REFERENCES

[1] H. B. Prajapati, J. P. Shah, and V. K. Dabhi, "Detection and classification of rice plant diseases," *Intelligent Decision Technologies*, vol. 11, no. 3, pp. 357–373, Jul. 2017.

[2] J. P. Shah, H. B. Prajapati, and V. K. Dabhi, "A survey on detection and classification of rice plant diseases," in *Proceedings of the 2016 IEEE International Conference on Current Trends in Advanced Computing (ICCTAC)*, Mar. 2016, pp. 1–8.

[3] K. Mondal, P. Dutta, and S. Bhattacharyya, "Efficient fuzzy rule base design using image features for image extraction and segmentation," in *2012 Fourth International Conference on Computational Intelligence and Communication Networks*, Nov. 2012, pp. 793–799.

[4] S. De, S. Bhattacharyya, and S. Chakraborty, "True color image segmentation by an optimized multilevel activation function," in *2010 IEEE International Conference on Computational Intelligence and Computing Research*, Dec. 2010, pp. 1–4.

[5] S. Kumar, R. Gupta, N. Khanna, S. Chaudhury, and S. D. Joshi, "Text extraction and document image segmentation using matched wavelets and MRF model," *IEEE Transactions on Image Processing*, vol. 16, no. 8, pp. 2117–2128, Aug. 2007.

[6] S. Shirgaonkar, D. H. Jeong, T. Huynh, and S. Ji, "Designing a robust bleeding detection method for brain CT image analysis," in *2012 IEEE International Conference on Bioinformatics and Biomedicine Workshops*, Oct. 2012, pp. 260–264.

[7] J. Lian, Y. Wang, and C. M. Akujuobi, "Dilation-3 PR QMF for image processing," in *2016 IEEE Southwest Symposium on Image Analysis and Interpretation (SSIAI)*, Mar. 2016, pp. 93–96.

[8] H. N. Saha, S. Tapadar, S. Ray, S. K. Chatterjee, and S. Saha, "A machine learning based approach for hand gesture recognition using distinctive feature extraction," in *2018 IEEE 8th Annual Computing and Communication Workshop and Conference (CCWC)*, Jan 2018, pp. 91–98.

[9] F. Iqbal, J. M. Hashmi, B. C. M. Fung, R. Batool, A. M. Khattak, S. Aleem, and P. C. K. Hung, "A hybrid framework for sentiment analysis using genetic algorithm based feature reduction," *IEEE Access*, vol. 7, pp. 14 637–14 652, 2019.

[10] H. H. Vo and A. Verma, "Discriminant color texture descriptors for diabetic retinopathy recognition," in *2016 IEEE 12th International Conference on Intelligent Computer Communication and Processing (ICCP)*, Sep. 2016, pp. 309–315.

[11] H. Qassim, A. Verma, and D. Feinzimer, "Compressed residual-VGG16 CNN model for big data places image recognition," in *2018 IEEE 8th Annual Computing and Communication Workshop and Conference (CCWC)*, Jan. 2018, pp. 169–175.

[12] P. Ly, D. Bein, and A. Verma, "New compact deep learning model for skin cancer recognition," in *2018 9th IEEE Annual Ubiquitous Computing, Electronics Mobile Communication Conference (UEMCON)*, Nov. 2018, pp. 255–261.

[13] M. I. U. Haque and D. Valles, "A facial expression recognition approach using DCNN for autistic children to identify emotions," in *2018 IEEE 9th Annual Information Technology, Electronics and Mobile Communication Conference (IEMCON)*, Nov. 2018, pp. 546–551.

[14] Q. Zhang, "Phase-domain deep patient-ECG image learning for zero-effort smart health security*," in *2019 41st Annual International Conference of the IEEE Engineering in Medicine and Biology Society (EMBC)*, Jul. 2019, pp. 2622–2628.

[15] P. Johnson and E. Abdelfattah, "Applying machine learning models to identify forest cover," in *2018 9th IEEE Annual Ubiquitous Computing, Electronics Mobile Communication Conference (UEMCON)*, Nov. 2018, pp. 471–474.

[16] A. Thomas, Y. Guo, Y. Kim, B. Aksanli, A. Kumar, and T. S. Rosing, "Hierarchical and distributed machine learning inference beyond the edge," in *2019 IEEE 16th International Conference on Networking, Sensing and Control (ICNSC)*, May 2019, pp. 18–23.

[17] G. Bajwa, M. Fazeen, R. Dantu, and S. Tanpure, "Unintentional bugs to vulnerability mapping in android applications," in *2015 IEEE International Conference on Intelligence and Security Informatics (ISI)*, May 2015, pp. 176–178.

[18] S. M. Alnaeli, A. D. A. Taha, and S. B. Binder, "Middleware and multi-core architecture: Challenges and potential enhancements from software engineering perspective," in *2016 IEEE International Conference on Electro Information Technology (EIT)*, May 2016, pp. 0700–0706.

[19] C. Jaiswal and V. Kumar, "DbHAaaS: Database high availability as a service," in *2015 11th International Conference on Signal-Image Technology Internet-Based Systems (SITIS)*, Nov. 2015, pp. 725–732.

[20] M. Beck, W. Hao, and A. Campan, "Accelerating the mobile cloud: Using amazon mobile analytics and k-means clustering," in *2017 IEEE 7th Annual Computing and Communication Workshop and Conference (CCWC)*, Jan. 2017, pp. 1–7.